

Development of an Oxygen Pressure Estimator Using the Immersion and Invariance Method for a Particular PEMFC System

Authors:

Ángel Hernández-Gómez, Víctor Ramirez, Belem Saldivar

Date Submitted: 2021-03-01

Keywords: sensor replacement, PEMFC system, non-linear system, Lyapunov's Theorem application, estimator development

Abstract:

The fault detection method has been used usually to give a diagnosis of the performance and efficiency in the proton exchange membrane fuel cell (PEMFC) systems. To be able to use this method a lot of sensors are implemented in the PEMFC to measure different parameters like pressure, temperature, voltage, and electrical current. However, despite the high reliability of the sensors, they can fail or give erroneous measurements. To address this problem, an efficient solution to replace the sensors must be found. For this reason, in this work, the immersion and invariance method is proposed to develop an oxygen pressure estimator based on the voltage, electrical current density, and temperature measurements. The estimator stability region is calculated by applying Lyapunov's Theorem and constraints to achieve stability are established for the oxygen pressure, electrical current density, and temperature. Under these estimator requirements, oxygen pressure measurements of high reliability are obtained to fault diagnosis without the need to use an oxygen sensor.

Record Type: Published Article

Submitted To: LAPSE (Living Archive for Process Systems Engineering)

Citation (overall record, always the latest version):

LAPSE:2021.0086

Citation (this specific file, latest version):

LAPSE:2021.0086-1

Citation (this specific file, this version):

LAPSE:2021.0086-1v1

DOI of Published Version: <https://doi.org/10.3390/pr8091095>

License: Creative Commons Attribution 4.0 International (CC BY 4.0)

Article

Development of an Oxygen Pressure Estimator Using the Immersion and Invariance Method for a Particular PEMFC System

Ángel Hernández-Gómez ^{1,†}, Víctor Ramirez ^{1,2,*,†}  and Belem Saldivar ^{2,3} 

¹ Department of Renewable Energy, Centro de Investigación Científica de Yucatán (CICY), Yucatán P.C. 97205, Mexico; angel.hernandez@cicy.mx

² Cátedras CONACYT, Ciudad de México P.C. 03940, Mexico; belemsaldivar@hotmail.com

³ Facultad de Ingeniería, Universidad Autónoma del Estado de México (UAEM), Toluca P.C. 50000, Mexico

* Correspondence: victor.ramirez@cicy.mx

† These authors contributed equally to this work.

Received: 28 July 2020; Accepted: 27 August 2020; Published: 3 September 2020



Abstract: The fault detection method has been used usually to give a diagnosis of the performance and efficiency in the proton exchange membrane fuel cell (PEMFC) systems. To be able to use this method a lot of sensors are implemented in the PEMFC to measure different parameters like pressure, temperature, voltage, and electrical current. However, despite the high reliability of the sensors, they can fail or give erroneous measurements. To address this problem, an efficient solution to replace the sensors must be found. For this reason, in this work, the immersion and invariance method is proposed to develop an oxygen pressure estimator based on the voltage, electrical current density, and temperature measurements. The estimator stability region is calculated by applying Lyapunov's Theorem and constraints to achieve stability are established for the oxygen pressure, electrical current density, and temperature. Under these estimator requirements, oxygen pressure measurements of high reliability are obtained to fault diagnosis without the need to use an oxygen sensor.

Keywords: estimator development; Lyapunov's Theorem application; non-linear system; PEMFC system; sensor replacement

1. Introduction

Fuel cell (FC) system is an advanced power system necessary for a clean, sustainable, and environmentally friendly future, because FCs are promising candidates as an alternative to conventional fossil fuels, due to their higher energy density, energy efficiency, and very low emissions [1–3]. The main operation of the FCs is to transform gaseous fuel chemical energy into electricity. Besides, the FCs can be used as alternative stationary and mobile power source [4,5]. The main types of FCs are proton exchange membrane, direct methanol, solid oxide, molten carbonate, phosphoric acid, alkaline, and microbial [6].

In particular, the proton exchange membrane fuel cell (PEMFC) has attracted the attention of researchers in the last few decades due to its characteristics as low operating temperature, low noise, quick start-up capability, light mass, and high-power density [2,4,6,7]. The PEMFCs have recently passed the test phase and have slightly reached the commercialization stage due to the impressive research effort [8]. However, the two biggest limitations preventing the PEMFC system from further commercialization are its reliability and durability [7].

A lot of studies on PEMFC performance have been carried out, since three-dimensional simulation models to more detailed measurement techniques, such as electrochemical impedance spectroscopy [9,10]. To have a PEMFC diagnosis, the fault detection method has been used commonly

to guarantee correct and safe operation in the PEMFC system [7,11,12]. However, to achieve such a diagnosis, several sensors have been used to measure different parameters like the mass flow, oxygen pressure, hydrogen pressure, compressor velocity, electrical current, water pressure, voltage, and temperature of the stack [11,13,14].

A lot of researchers have worked on the development of sensors with high reliability [15–18]. These devices must present characteristics, such as high sensitivity and selectivity, robustness, fast response time, operation at high temperature and low power consumption [19–21]. However, in real applications, the reliability of sensors during the system operation is variable. Thus, inaccurate sensor measurements can provide misleading results in PEMFC fault diagnosis, which can end in failures and damages of the PEMFC system [7,11]. To solve this problem, novel methods have been proposed to reduce errors in PEMFC fault diagnosis [9,10]. For this reason, an efficient method to replace the oxygen sensor is proposed in this work, since the oxygen management system is an important subsystem, which is used for supplying proper oxygen pressure in the PEMFC stack cathode. Besides, the complexity and nonlinearity of the oxygen pressure are difficult to model [22]. So, using the voltage, electrical current density, and temperature measurements and applying the immersion and invariance (gradient estimator) method it is possible to develop an oxygen pressure estimator for getting high-reliability oxygen measurements avoiding the use of oxygen sensor for PEMFC system fault diagnosis.

The paper is organized as follows, the formulation of a gradient estimator to develop the oxygen pressure estimator is described in Section 2. The PEMFC potential-current behavior is discussed in Section 3. The oxygen pressure estimator applied to a PEMFC system is presented in Section 4. The simulation and results are introduced in Section 5. Finally, some concluding remarks are presented in Section 6.

2. Formulation of Gradient Estimator

The immersion and invariance (gradient estimator) method has been proposed to solve problems of stabilization and adaptive control of nonlinear systems, which are present in any real practical problem [23–26]. The key step for the estimator development using this method is the construction of a monotone mapping, which explicitly depends on some of the estimator tuning parameters [27,28]. For these reasons, in this work, this method has been used to develop the oxygen pressure estimator.

The estimator design is formulated by proposing a function where the system behavior representation distinguishes between measurable and not measurable signals. As shown in [28,29], there is a general kind of function dependent on two variables θ and ξ expressed by

$$F(\theta, \xi) = G(\theta) + H(\xi) + K(\theta, \xi) \quad (1)$$

with $\theta > 0$ and $\xi > 0$, where ξ and θ are known and time-dependent variables, such that measurable signals $F(\theta, \xi)$ and $H(\xi)$ are represented by

$$y(t) = F(\theta, \xi) - H(\xi). \quad (2)$$

Indeed, the representation in the non-linear regression form will be

$$y(t) = \phi(\theta, \xi), \quad (3)$$

where

$$\phi(\theta, \xi) := G(\theta) + K(\theta, \xi). \quad (4)$$

Given this formulation, the following proposition can be stated.

Proposition 1. Consider the function $\phi(\theta, \xi)$, where $F(\theta, \xi)$ and $H(\xi)$ are known and the variable corresponding to the non-linear regression model satisfies that the partial derivative of $\phi(\theta, \xi)$ with respect to θ is greater than zero. Then, the gradient estimator is given by

$$\hat{\theta} = \gamma(y(t) - \phi(\hat{\theta}, \xi)) \quad (5)$$

with $\gamma > 0$ ensuring that

$$\lim_{t \rightarrow \infty} \hat{\theta} = \theta, \quad (6)$$

for all initial condition $\hat{\theta}_0$ such as $\frac{\partial \phi(\hat{\theta}_0, \xi)}{\partial \theta} > 0$.

Proof. To show that the immersion and invariance estimator converges to the desired value, it is necessary to use the monotonicity property of the function $\phi(\theta, \xi)$ concerning θ . Then, as:

$$\frac{\partial \phi(\theta, \xi)}{\partial \theta} > 0, \quad (7)$$

the function is strictly monotonically increasing and also fulfills

$$(\hat{\theta} - \theta) [\phi(\hat{\theta}, \xi) - \phi(\theta, \xi)] > 0 \quad \forall \hat{\theta} \neq \theta, \quad (8)$$

taking the Lyapunov's function candidate

$$V(\hat{\theta}) = \frac{1}{2\gamma} (\hat{\theta} - \theta)^2, \quad (9)$$

its time-derivative along the trajectories of (2)–(5) is given by

$$\dot{V} = -(\hat{\theta} - \theta) [\phi(\hat{\theta}, \xi) - \phi(\theta, \xi)] < 0 \quad \forall \hat{\theta} \neq \theta. \quad (10)$$

Note that the negative definiteness of \dot{V} immediately follows from (8). Then, the proof is completed by using Lyapunov's Second Stability Theorem. \square

3. PEMFC Potential-Current Behavior

An accurate mathematical model to represent the PEMFC potential V_c has been reported in [30], where V_c is a depending function of stack current, cathode pressure, reactant partial pressures, PEMFC temperature, and membrane humidity using a combination of physical and empirical relationships, and can be expressed in terms of the Nernst's potential E_{th} and the three main types of potential drops; activation V_{act} , ohmic V_{ohm} , and concentration V_{con} .

$$V_c(\theta, \xi) = E_{th}(\theta) - V_{ohm}(\xi) - V_{act}(\theta, \xi) - V_{con}(\theta, \xi), \quad (11)$$

where θ denotes the oxygen pressure (*atm*), and ξ the electrical current density in the cell ($A \cdot \text{cm}^{-2}$). Nernst's potential E_{th} . The Nernst's potential or open-circuit potential is the maximum power obtained by one cell corresponding to exchange Gibbs free energy as a result of the difference between reactant products and Gibbs's free energy. It can be described by the following equation [30–32].

$$E_{th}(\theta) = E_0 + B_1(T_0 - T) + B_2 T \ln \left[\frac{P_{H_2} \theta^{1/2}}{P_{H_2O}} \right], \quad (12)$$

where T_0 and T are the initial temperature and the cell temperature, respectively (*K*), P_{H_2} is a positive constant that represents the hydrogen pressure (*atm*), and E_0 is the reference potential (*V*). B_1 and B_2

are positive constants that depend on stack temperature and potential (V/K) [30]. Water pressure is represented by P_{H_2O} (*atm*).

Ohmic potential drop V_{ohm} . The ohmic potential drop arises from the resistance of the polymer membrane to the transfer of protons and from the resistance of the electrode and the collector plate to the transfer of electrons [30–32].

$$V_{ohm}(\xi) = \frac{\xi}{A_{fc}} R_{ohm}, \quad (13)$$

where $R_{ohm} > 0$ is the internal electrical resistance (Ω) and A_{fc} is the cell active area. Besides, the ohmic resistance can be expressed as a function of the membrane conductivity ($\text{cm}^{-1} \cdot \Omega^{-1}$), σ_m .

$$R_{ohm} = \frac{t_m}{\sigma_m}, \quad (14)$$

where t_m is the thickness of the membrane (*cm*), and σ_m is a function of membrane water content λ_m and the cell temperature T .

$$\sigma_m = b_1 \exp \left[b_2 \left(\frac{1}{303} - \frac{1}{T} \right) \right], \quad (15)$$

where b_1 is a function of membrane water content and b_2 is a constant [30].

$$b_1 = b_{11} \lambda_m - b_{12}, \quad (16)$$

where b_2 , b_{11} , and b_{12} are usually determined empirically. In this work, the values for b_2 , b_{11} , and b_{12} are taken from [33].

Activation potential drop V_{act} . The activation potential drop comes when the movement of electrons needs to break and form chemical bonds in the anode and cathode (i.e., part of the available energy is lost in driving the chemical reaction that transfers the electrons to and from the electrodes). Although the activation overvoltage occurs at both PEMFC electrodes, the reaction of hydrogen oxidation at the anode is faster than the reaction of oxygen [30–32].

$$V_{act}(\theta) = V_o + V_a(\theta)(1 - \exp[-c_1 \xi]), \quad (17)$$

where c_1 is a constant. The functions V_o and V_a are both dependent on oxygen pressure and temperature. They have been calculated empirically by

$$V_o = V_o^0 + B_1(T_0 - T) - 1.07551B_2T + \frac{3B_2T}{2} \ln \left(\frac{P_{ca} - P_{sat}}{P_{atm}} \right), \quad (18)$$

where V_o^0 is the initial potential drop (V) at zero current density. P_{ca} and P_{atm} are the pressures of the cathode and atmospheric, respectively (*atm*). The water saturation pressure P_{sat} (*mPa*) is expressed as

$$\log_{10} P_{sat} = \frac{-1.69}{10^{10}} T^4 + \frac{3.85}{10^7} T^3 - \frac{3.39}{10^4} T^2 + 0.143T - 20.92. \quad (19)$$

The function V_a is given as:

$$V_a(\theta) = B_3 \left(\frac{\theta}{0.1173} + P_{sat} \right)^2 + B_4 \left(\frac{\theta}{0.1173} + P_{sat} \right) + B_5, \quad (20)$$

where the constants B_3 , B_4 , and B_5 are dependent on the stack temperature and the voltage (V/K) and usually are determined empirically [30].

Concentration of potential drop V_{con} . The concentration of potential drop corresponds to the concentration gradients formed due to mass diffusions from the flow channels to the reaction sites (catalyst area). The factors underlying this potential drop are high current densities, slow transportation of reactants and products, and water film covering the catalyst surfaces to the anode and cathode [30–32].

$$V_{con}(\theta, \xi) = \xi \left(\frac{c_2 \xi}{I_{max}} \right)^{c_3}, \quad (21)$$

where $c_3 \in \mathbb{R}_+$ is a constant, I_{max} is the maximum electrical current density in the cell and c_2 is an oxygen pressure function [30].

$$c_2 = \begin{cases} B_6 \left(\frac{\theta}{0.1173} + P_{sat} \right) + B_7 & \text{if } h(\theta) < 0, \\ B_8 \left(\frac{\theta}{0.1173} + P_{sat} \right) + B_9 & \text{if } h(\theta) \geq 0, \end{cases} \quad (22)$$

where

$$h(\theta) = \theta + 0.1173P_{sat} - 0.2346 \text{ atm},$$

and B_6 , B_7 , B_8 , and B_9 are constant values that depend on the stack temperature and are usually determined empirically.

Lemma 1. The discontinuous function c_2 defined in (22) can be approximated by the continuous function C_2 given below.

$$C_2 = D_1 \left(\frac{\theta}{0.1173} + P_{sat} \right) + D_2, \quad (23)$$

where

$$D_1 = \frac{1}{2}B_6 + \frac{1}{2}B_8 + \frac{1}{2}(B_6 - B_8) \tanh[h(\theta)],$$

and

$$D_2 = \frac{1}{2}B_7 + \frac{1}{2}B_9 + \frac{1}{2}(B_7 - B_9) \tanh[h(\theta)].$$

The parameters values of the PEMFC voltage model are taken from [30] (see Table 1).

Table 1. Parameters for the PEMFC voltage model [30].

Symbol	Parameter	Value
A_{fc}	Cell Active Area	100 cm ²
E_0	Reference Potential	1229 × 10 ⁻³ V
I_{max}	Maximum Current Density	2.2 A · cm ⁻²
P_{atm}	Atmospheric Pressure	1 atm
P_{ca}	Cathode Pressure	2 atm
P_{H_2}	Hydrogen Pressure	1 atm
P_{H_2O}	Water Pressure	396 × 10 ⁻³ atm
t_m	Membrane Thickness	125 × 10 ⁻⁴ cm
T_0	Initial Temperature	298.15 K
V_o^0	Initial Potential Drop	279 × 10 ⁻³ V
b_1	Membrane Humidity Function	686 × 10 ⁻⁴ cm ⁻¹ · Ω ⁻¹
b_2	Constant	350 K
b_{11}	Constant	513 × 10 ⁻⁵ SO ₃ ⁻ · H ₂ O ⁻¹ · cm ⁻¹ · Ω ⁻¹

Table 1. Cont.

Symbol	Parameter	Value
b_{12}	Constant	$326 \times 10^{-5} \text{cm}^{-1} \cdot \Omega^{-1}$
c_1	Constant	10A^{-1}
c_3	Constant	2 (-)
B_1	Temperature and Potential Function	$85 \times 10^{-5} \text{V} \cdot \text{K}^{-1}$
B_2	Temperature and Potential Function	$43085 \times 10^{-6} \text{V} \cdot \text{K}^{-1}$
B_3	Temperature and Potential Function	$-1618 \times 10^{-8} \text{T} \cdot \text{V} \cdot \text{K}^{-1} + 1618 \times 10^{-5} \text{V}$
B_4	Temperature and Potential Function	$18 \times 10^{-4} \text{T} \cdot \text{V} \cdot \text{K}^{-1} - 166 \times 10^{-3} \text{V}$
B_5	Temperature and Potential Function	$-58 \times 10^{-5} \text{T} \cdot \text{V} \cdot \text{K}^{-1} + 5736 \times 10^{-4} \text{V}$
B_6	Temperature Function	$358 \times 10^{-5} \text{T} \cdot \text{K}^{-1} - 622 \times 10^{-3}$
B_7	Temperature Function	$-725 \times 10^{-6} \text{T} \cdot \text{K}^{-1} + 1.68$
B_8	Temperature Function	$433 \times 10^{-6} \text{T} \cdot \text{K}^{-1} - 68 \times 10^{-3}$
B_9	Temperature Function	$-8 \times 10^{-4} \text{T} \cdot \text{K}^{-1} + 54 \times 10^{-2}$
λ_m	Membrane Humidity	$14 \text{H}_2\text{O} \cdot (\text{SO}_3^-)^{-1}$

4. Application of Oxygen Pressure Estimator to a PEMFC System

The oxygen pressure estimator presented in this section is derived from the results presented in Sections 2 and 3. The measurable signal is defined by applying the Equations (2)–(11).

$$y(t) = V_c(\theta, \xi) + V_{ohm}(\xi), \quad (24)$$

where

$$\phi(\theta, \xi) := E_{th}(\theta) - V_{act}(\theta, \xi) - V_{con}(\theta, \xi). \quad (25)$$

Now a proposition related to the PEMFC system is presented.

Proposition 2. Consider the function $\phi(\theta, \xi)$, with C_2 and θ are greater than zero, such that, inequality (26) is satisfied

$$B_2 T (P_{ca} - P_{sat} - 3\theta) - 2 \left(\frac{\partial V_a}{\partial \theta} \right) \theta (P_{ca} - P_{sat}) \geq 0. \quad (26)$$

Then, ξ can be expressed in terms of θ and T as follows:

$$\xi = \left(D \left[\frac{B_2 T}{2} \left(\frac{P_{ca} - P_{sat} - 3\theta}{\theta(P_{ca} - P_{sat})} \right) - \frac{\partial V_a}{\partial \theta} \right] \right)^{\frac{1}{c_3 + 1}}, \quad (27)$$

where

$$D = \frac{I_{max}^{c_3}}{c_3 C_2^{c_3 - 1}} \left(\frac{\partial C_2}{\partial \theta} \right)^{-1}$$

and $\frac{\partial \phi(\theta, \xi)}{\partial \theta} > 0$.

Proof. The proof starts with the partial derivative of ϕ with respect to θ , which is given by

$$\frac{\partial \phi(\theta, \xi)}{\partial \theta} = \frac{B_2 T}{2} \left(\frac{P_{ca} - P_{sat} - 3\theta}{\theta(P_{ca} - P_{sat})} \right) - \frac{\partial V_a}{\partial \theta} (1 - \exp[-c_1 \xi]) - \frac{\partial C_2}{\partial \theta} \left(\frac{c_3 C_2^{c_3 - 1} \xi^{c_3 + 1}}{I_{max}^{c_3}} \right).$$

Now, taking the set of values (θ, ξ) , that satisfy inequality (28),

$$0 \leq \frac{B_2 T}{2} \left(\frac{P_{ca} - P_{sat} - 3\theta}{\theta(P_{ca} - P_{sat})} \right) - \frac{\partial V_a}{\partial \theta} (1 - \exp[-c_1 \xi]) - \frac{\partial C_2}{\partial \theta} \left(\frac{c_3 C_2^{c_3-1} \xi^{c_3+1}}{I_{max}^{c_3}} \right). \tag{28}$$

Since $0 < 1 - \exp[-c_1 \xi] < 1$ for ξ and $c_1 > 0$, then

$$0 \leq \frac{B_2 T}{2} \left(\frac{P_{ca} - P_{sat} - 3\theta}{\theta(P_{ca} - P_{sat})} \right) - \frac{\partial V_a}{\partial \theta} - \frac{\partial C_2}{\partial \theta} \left(\frac{c_3 C_2^{c_3-1} \xi^{c_3+1}}{I_{max}^{c_3}} \right) < \frac{\partial \phi(\theta, \xi)}{\partial \theta}.$$

So, the admissible limit values (θ, ξ) that satisfy inequality (28) can be found when this is equal to zero.

$$0 = \frac{B_2 T}{2} \left(\frac{P_{ca} - P_{sat} - 3\theta}{\theta(P_{ca} - P_{sat})} \right) - \frac{\partial V_a}{\partial \theta} - \frac{\partial C_2}{\partial \theta} \left(\frac{c_3 C_2^{c_3-1} \xi^{c_3+1}}{I_{max}^{c_3}} \right),$$

setting

$$D = \frac{I_{max}^{c_3}}{c_3 C_2^{c_3-1}} \left(\frac{\partial C_2}{\partial \theta} \right)^{-1},$$

thus,

$$\xi = \left(D \left[\frac{B_2 T}{2} \left(\frac{P_{ca} - P_{sat} - 3\theta}{\theta(P_{ca} - P_{sat})} \right) - \frac{\partial V_a}{\partial \theta} \right] \right)^{\frac{1}{c_3 + 1}}.$$

As $\frac{\partial C_2}{\partial \theta} > 0$, then,

$$\frac{B_2 T}{2} \left(\frac{P_{ca} - P_{sat} - 3\theta}{\theta(P_{ca} - P_{sat})} \right) - \frac{\partial V_a}{\partial \theta} \geq 0,$$

since $\theta > 0$ and $P_{ca} - P_{sat} > 0$, then,

$$B_2 T(P_{ca} - P_{sat} - 3\theta) - 2 \left(\frac{\partial V_a}{\partial \theta} \right) \theta(P_{ca} - P_{sat}) \geq 0.$$

□

Now the following proposition is introduced as a result of the combination of Proposition 1 and Proposition 2. This result shows the estimator and its stability using Lyapunov’s functions.

Proposition 3. Consider the function $\phi(\theta, \xi)$, C_2 and θ are greater than zero, such that, inequality (26) is satisfied and with ξ expressed as:

$$\xi = \left(D \left[\frac{B_2 T}{2} \left(\frac{P_{ca} - P_{sat} - 3\theta}{\theta(P_{ca} - P_{sat})} \right) - \frac{\partial V_a}{\partial \theta} \right] \right)^{\frac{1}{c_3 + 1}}.$$

Then, the gradient estimator of oxygen pressure is given by

$$\hat{\theta} = \gamma(y(t) - \phi(\hat{\theta}, \xi)), \tag{29}$$

with $\gamma > 0$, ensuring that

$$\lim_{t \rightarrow \infty} \hat{\theta} = \theta. \tag{30}$$

Proof. For the values of θ and ξ stated in the hypothesis of Proposition 2, it is obtained that the partial derivative of $\phi(\theta, \xi)$ with respect to θ is greater than zero. Then, by Proposition 1, the gradient estimator of oxygen pressure is given by

$$\dot{\hat{\theta}} = \gamma(y(t) - \phi(\hat{\theta}, \xi)),$$

with $\gamma > 0$, ensuring that

$$\lim_{t \rightarrow \infty} \hat{\theta} = \theta.$$

□

5. Simulations and Results

The Runge–Kutta fourth-order algorithm, described in [34], and the values of the parameters given in the Table 1 were used to perform the simulations. The first step was to determine the stability region for the estimator under the established constraints of the Propositions 2 and 3. The estimator stability region is given within the interval (0 atm, 0.45 atm) and the simulation results of such constraints are shown in Figures 1 and 2. The behavior of the partial derivative of ϕ with respect to θ as a function of θ and ξ for different temperatures is shown in Figure 1.

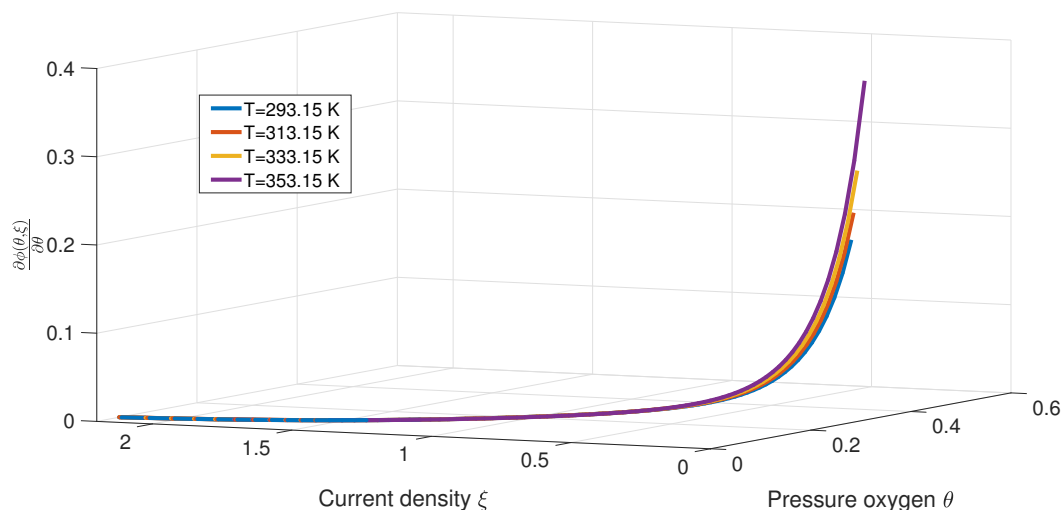


Figure 1. Behavior of the partial derivative of ϕ concerning θ .

The behavior of θ and ξ considering the established constraints for different temperatures is shown in Figure 2.

Within stability region, the oxygen pressure estimator and the PEMFC potential-current simulations were performed using oxygen pressure equal to 0.3 atm and different values for θ_0 and γ . The oxygen pressure estimator shows an asymptotic convergence to the proposed value for oxygen pressure. The estimator behavior can be appreciated for different values θ_0 in Figure 3, and different values of γ in Figure 4.

The electrical current density calculated based on the estimator proved an asymptotic convergence to the electrical current density calculated for oxygen pressure equal to 0.3 atm, the simulation is shown for different values of θ_0 in Figure 5, and for different values of γ in Figure 6.

The cell potential calculated based on the estimator evidenced an asymptotic convergence to the potential calculated for oxygen pressure equal to 0.3 atm, the simulation results for different values of θ_0 are shown in Figure 7 and for different values of γ in Figure 8.

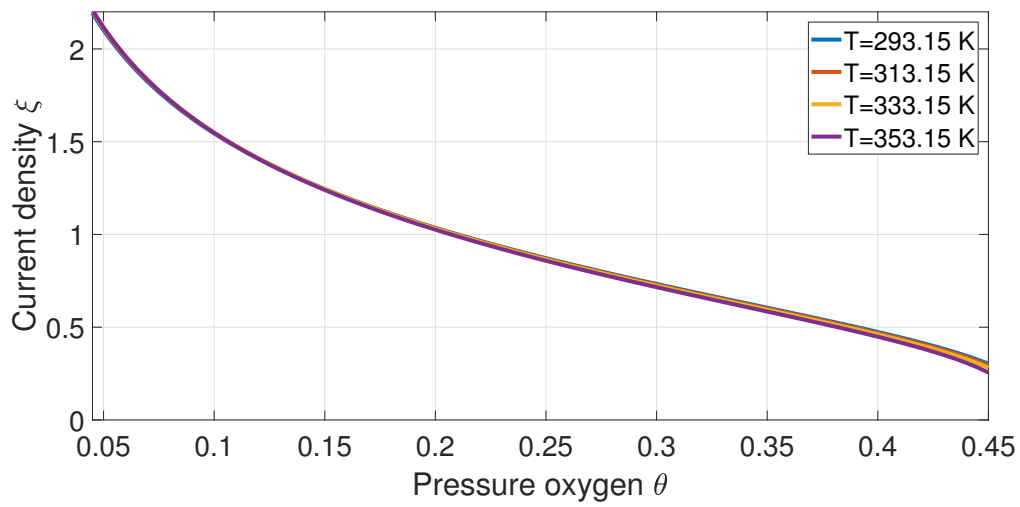


Figure 2. Behavior of the partial derivative of ϕ concerning θ .

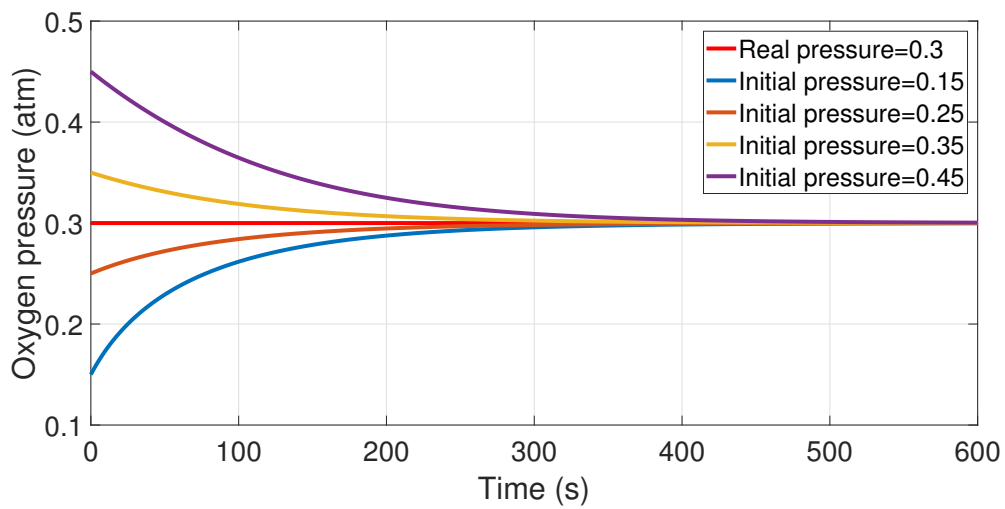


Figure 3. Estimator behavior with different values θ_0 .

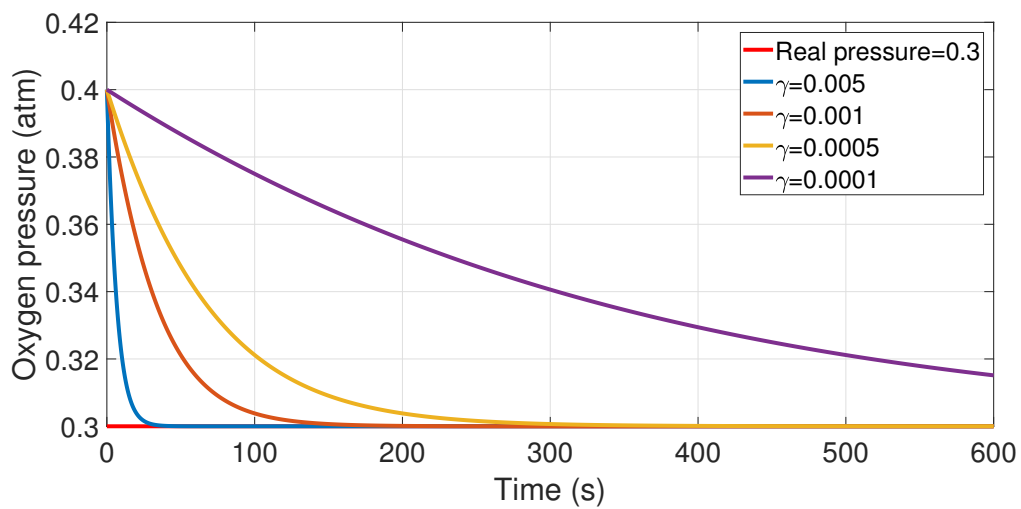


Figure 4. Estimator behavior with different values γ .

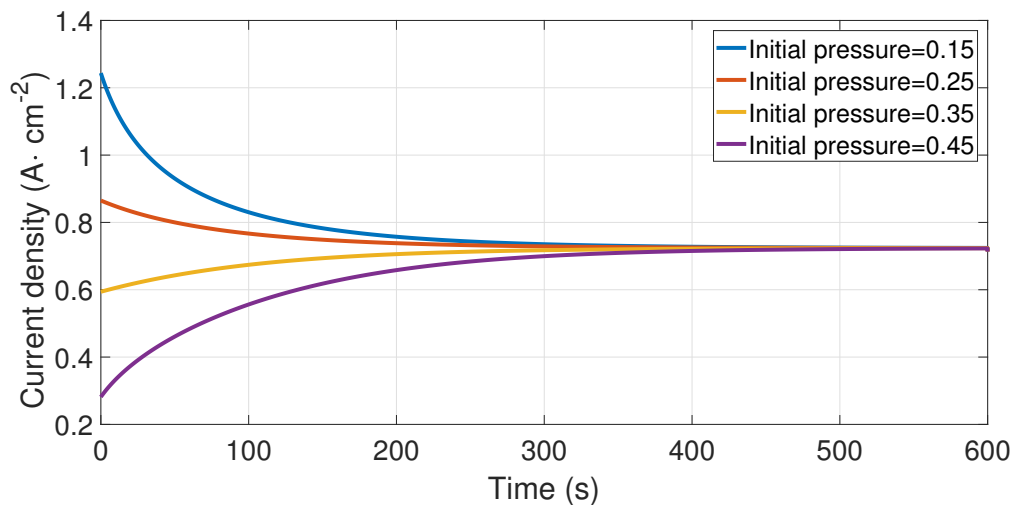


Figure 5. Simulation of electrical current density stability with different values θ_0 .

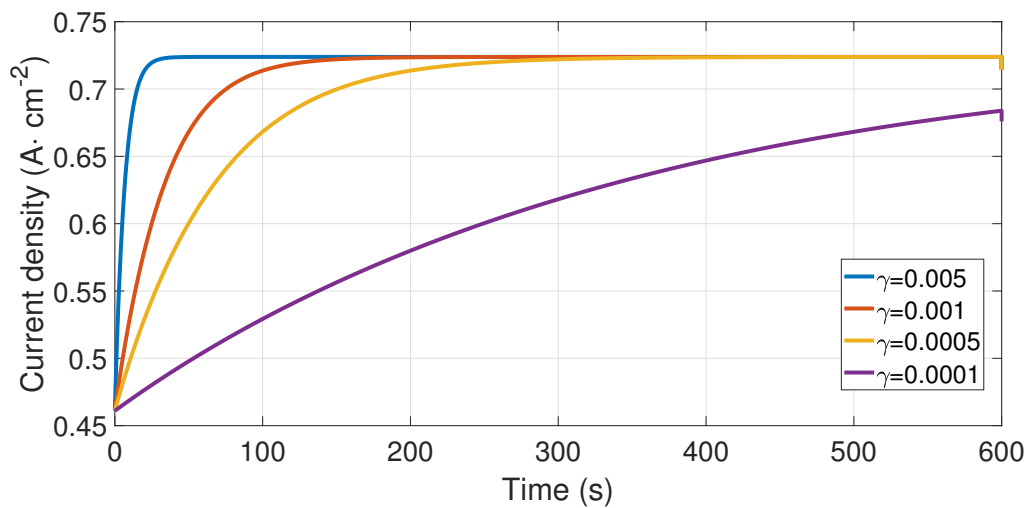


Figure 6. Simulation of electrical current density stability with different values γ .

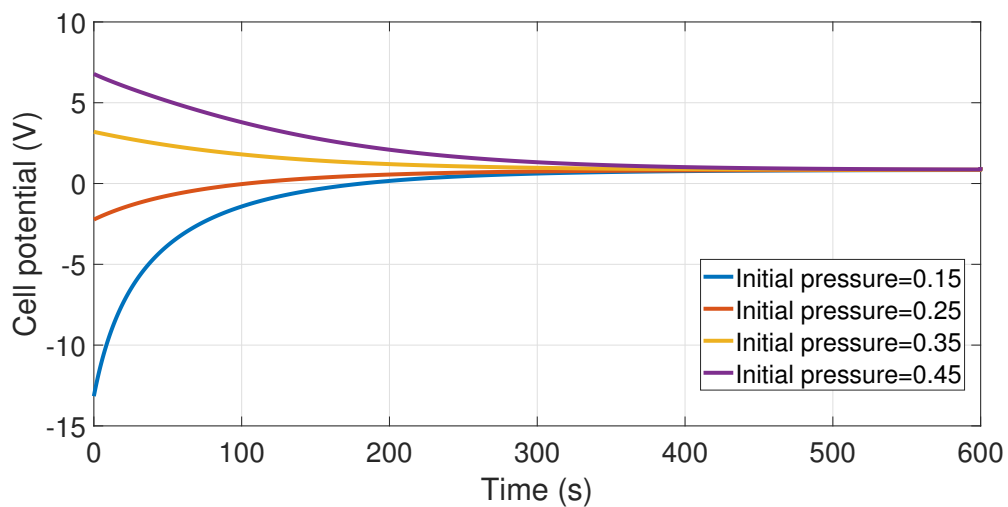


Figure 7. Simulation of potential stability with different values θ_0 .

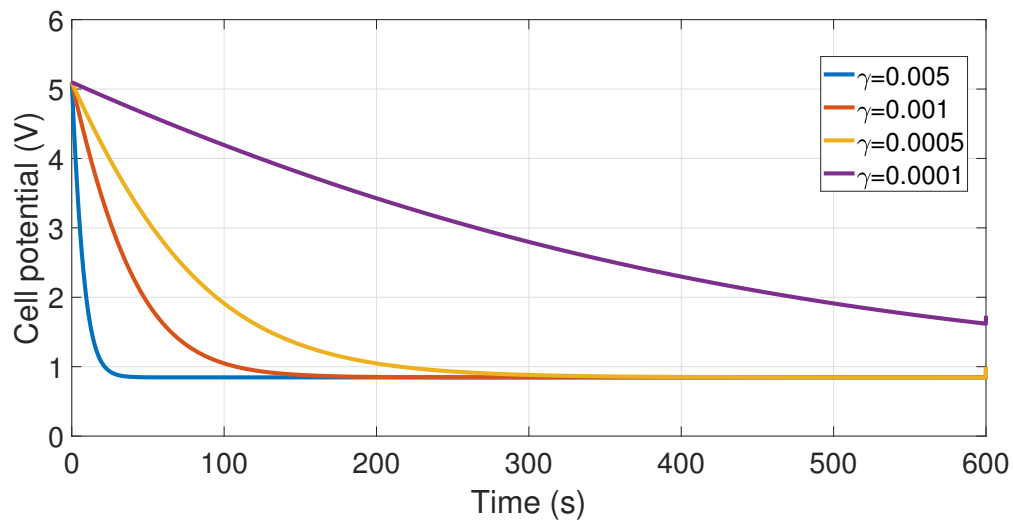


Figure 8. Simulation of potential stability with different values γ .

Finally, the power or potential-current performance curve based on the estimator demonstrated an asymptotic convergence to the power for oxygen pressure equal to 0.3 atm, the simulation is shown for different values of θ_0 in Figure 9, and for different values of γ in Figure 10. This curve has proved to be of vital importance for the PEMFC system fault diagnosis [35].

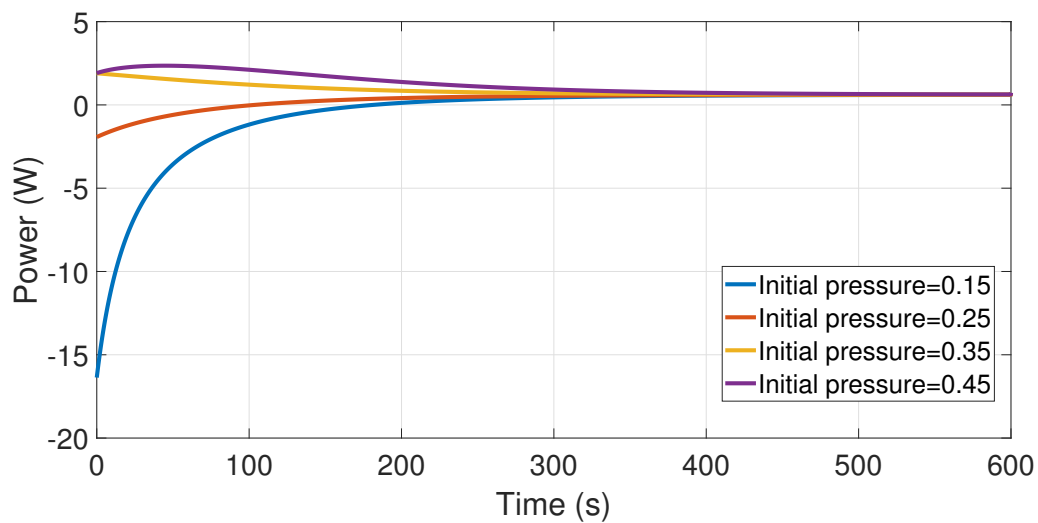


Figure 9. Simulation of power stability with different values θ_0 .

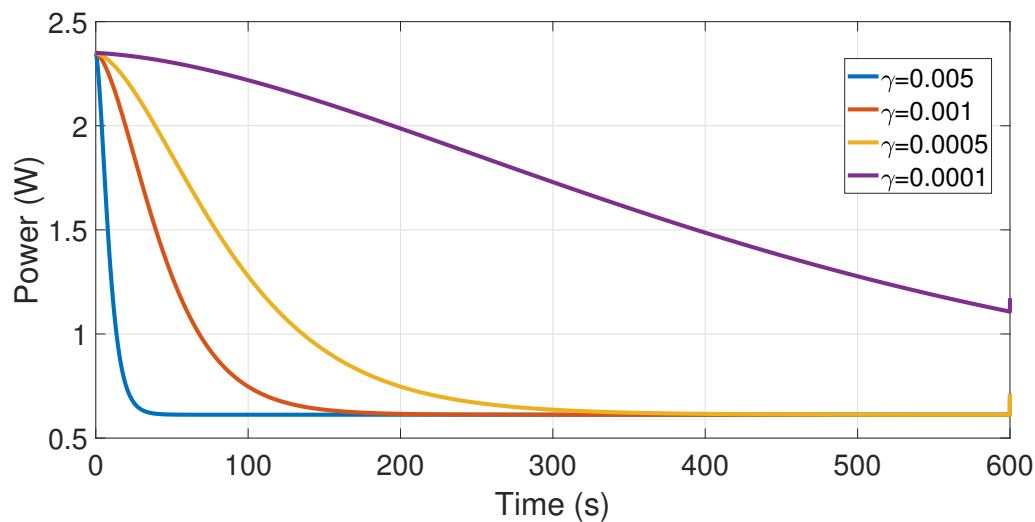


Figure 10. Simulation of power stability with different values γ .

6. Conclusions

To avoid oxygen sensors for PEMFCs, an oxygen pressure estimator has been developed based on the immersion and invariance (gradient estimator) method, and its stability conditions are established using Lyapunov's Theorem. Additionally, in this work, the PEMFC electrical current density has been characterized in terms of oxygen pressure and temperature under certain constraints.

The oxygen pressure estimator presents an absolute convergence within the stability region to the measurable value of oxygen pressure. However, the corresponding working condition can be different because it is directly related to laboratory environmental conditions. So, the next step is to evaluate the performance of the proposed estimator under different PEMFC conditions to improve the oxygen pressure estimator.

Author Contributions: Conceptualization, Á.H.-G. and V.R.; methodology, V.R.; software, Á.H.-G.; validation, Á.H.-G. and V.R.; formal analysis, Á.H.-G.; investigation, Á.H.-G. and V.R.; resources, V.R.; writing—original draft preparation, Á.H.-G. and V.R.; writing—review and editing, Á.H.-G., V.R., and B.S.; visualization, Á.H.-G.; supervision, V.R.; project administration, V.R.; funding acquisition, V.R. All authors have read and agreed to the published version of the manuscript.

Funding: This work has been supported by CONACyT-Mexico under the project 2015-01-786 (National Problems).

Acknowledgments: Thanks to the CONACyT-Mexico program Becas Nacional (Tradicional) 2018–2 and the scholarship 2018–000068–02NACF.

Conflicts of Interest: The authors declare no conflict of interest.

References

- Sopian, K.; Daud, W.R.W. Challenges and future developments in proton exchange membrane fuel cells. *Renew. Energy* **2006**, *31*, 719–727. [[CrossRef](#)]
- Shen, M.; Scott, K. Power loss and its effect on fuel cell performance. *J. Power Sources* **2005**, *148*, 24–31. [[CrossRef](#)]
- Leonardi, S.G.; Bonavita, A.; Donato, N.; Neri, G. Development of a hydrogen dual sensor for fuel cell applications. *Int. J. Hydrogen Energy* **2018**, *43*, 11896–11902. [[CrossRef](#)]
- Pukrushpan, J.T.; Stefanopoulou, A.G.; Peng, H. Chapter one-background and introduction. In *Control Fuel Cell Power System; Advances in Industrial Control*; Grimbale, M.J., Johnson, M.A., Eds.; Springer: London, UK, 2004; pp. 1–13. [[CrossRef](#)]
- Larminie, J.; Dicks, A. *Fuel Cell Systems Explained*, 2nd ed.; John Wiley & Sons, Ltd.: Chichester, UK, 2013; Chapter 1, pp. 1–24. [[CrossRef](#)]

6. Daud, W.; Rosli, R.; Majlan, E.; Hamid, S.; Mohamed, R.; Husaini, T. PEM fuel cell system control: A review. *Renew. Energy* **2017**, *113*, 620–638. [[CrossRef](#)]
7. Mao, L.; Jackson, L.; Huang, W.; Li, Z.; Davies, B. Polymer electrolyte membrane fuel cell fault diagnosis and sensor abnormality identification using sensor selection method. *J. Power Sources* **2020**, *447*, 227394. [[CrossRef](#)]
8. Wee, J.-H. Applications of proton exchange membrane fuel cell systems. *Renew. Sustain. Energy Rev.* **2007**, *11*, 1720–1738. [[CrossRef](#)]
9. Zhang, X.; Zhou, J.; Chen, W. Data-driven fault diagnosis for PEMFC systems of hybrid tram based on deep learning. *Int. J. Hydrogen Energy* **2020**, *45*, 13483–13495. [[CrossRef](#)]
10. Abbaspour, A.; Yen, K.K.; Forouzannezhad, P.; Sargolzaei, A. An Adaptive Resilient Control Approach for Pressure Control in Proton Exchange Membrane Fuel Cells. *IEEE Trans. Ind. Appl.* **2019**, *55*, 6344–6354. [[CrossRef](#)]
11. Li, S.; Aitouche, A.; Wang, H.; Christov, N. Sensor fault estimation of PEM fuel cells using Takagi Sugeno fuzzy model. *Int. J. Hydrogen Energy* **2020**, *45*, 11267–11275. [[CrossRef](#)]
12. Zheng, Z.; Petrone, R.; Péra, M.-C.; Hissel, D.; Becherif, M.; Pianese, C.; Steiner, N.Y.; Sorrentino, M. A review on non-model based diagnosis methodologies for PEM fuel cell stacks and systems. *Int. J. Hydrogen Energy* **2013**, *38*, 8914–8926. [[CrossRef](#)]
13. Higgins, S.R.; Ewan, J.; St-Pierre, J.; Severa, G.; Davies, K.; Bethune, K.; Goodarzi, A.; Rocheleau, R. Environmental sensor system for expanded capability of PEM fuel cell use in high air contaminant conditions. *Int. J. Hydrogen Energy* **2018**, *43*, 22584–22594. [[CrossRef](#)]
14. Arama, F.Z.; Mammari, K.; Laribi, S.; Necaibia, A.; Ghaitaoui, T. Implementation of sensor based on neural networks technique to predict the PEM fuel cell hydration state. *J. Energy Storage* **2020**, *27*, 101051. [[CrossRef](#)]
15. Jung, S.-W.; Lee, E.K.; Kim, J.H.; Lee, S.-Y. High-concentration nafion-based hydrogen sensor for fuel-cell electric vehicles. *Solid State Ion.* **2020**, *344*, 115134. [[CrossRef](#)]
16. Xiao, N.; Wu, R.; Huang, J.J.; Selvaganapathy, P.R. Development of a xurographically fabricated miniaturized low-cost, high-performance microbial fuel cell and its application for sensing biological oxygen demand. *Sens. Actuators Chem.* **2019**, 127432. [[CrossRef](#)]
17. Lee, C.-Y.; Lin, J.-T.; Chen, C.-H.; Lee, S.-J.; Wang, Y.-S. Development of a four-in-one sensor for low temperature fuel cell. *Renew. Energy* **2019**, *135*, 1452–1465. [[CrossRef](#)]
18. He, L.; Liu, Q.; Zhang, S.; Zhang, X.; Gong, C.; Shu, H.; Wang, G.; Liu, H.; Wen, S.; Zhang, B. High sensitivity of TiO₂ nanorod array electrode for photoelectrochemical glucose sensor and its photo fuel cell application. *Electrochem. Commun.* **2018**, *94*, 18–22. [[CrossRef](#)]
19. Montpart, N.; Baeza, M.; Baeza, J.A.; Guisasola, A. Low-cost fuel-cell based sensor of hydrogen production in lab scale microbial electrolysis cells. *Int. J. Hydrogen Energy* **2016**, *41*, 20465–20472. [[CrossRef](#)]
20. Lavanya, N.; Sekar, C.; Fazio, E.; Neri, F.; Leonardi, S.; Neri, G. Development of a selective hydrogen leak sensor based on chemically doped SnO₂ for automotive applications. *Int. J. Hydrogen Energy* **2017**, *42*, 10645–10655. [[CrossRef](#)]
21. Hayakawa, I.; Iwamoto, Y.; Kikuta, K.; Hirano, S. Gas sensing properties of platinum dispersed-TiO₂ thin film derived from precursor. *Sens. Actuators Chem.* **2000**, *62*, 55–60. [[CrossRef](#)]
22. Yang, D.; Wang, Y.; Chen, Z. Robust fault diagnosis and fault tolerant control for PEMFC system based on an augmented LPV observer. *Int. J. Hydrog. Energy* **2020**, *45*, 13508–13522. [[CrossRef](#)]
23. Astolfi, A.; Ortega, R. Immersion and invariance: A new tool for stabilization and adaptive control of nonlinear systems. *IEEE Trans. Autom. Control.* **2003**, *48*, 590–606. [[CrossRef](#)]
24. Hu, J.; Zhang, H. Immersion and invariance based command-filtered adaptive backstepping control of VTOL vehicles. *Automatica* **2013**, *49*, 2160–2167. [[CrossRef](#)]
25. Zhu, R.; Wang, H.; Yin, G.; Ding, Z. High performance nonlinear adaptive control of temperature in cryogenic wind tunnel. *Int. J. Robust Nonlinear Control* **2019**, *25*, 5118–5136. [[CrossRef](#)]
26. Ortega, R.; Nikiforov, V.; Gerasimov, D. On modified parameter estimators for identification and adaptive control, A unified framework and some new schemes. *Annu. Rev. Control.* **2020**. [[CrossRef](#)]
27. Liu, X.; Ortega, R.; Su, H.; Chu, J. Immersion and invariance adaptive control of nonlinearly parameterized nonlinear systems. *IEEE Trans. Autom. Control* **2010**, *55*, 2209–2214. [[CrossRef](#)]
28. Ortega, R.; Liu, X.; Su, H.; Chu, J. Immersion and invariance adaptive control of nonlinearly parameterized nonlinear systems *. *IFAC Proc. Vol.* **2010**, *43*, 641–646. [[CrossRef](#)]

29. Liu, X.; Ortega, R.; Su, H.; Chu, J. On adaptive control of nonlinearly parameterized nonlinear systems: Towards a constructive procedure. *Syst. Control Lett.* **2011**, *60*, 36–43. [[CrossRef](#)]
30. Pukrushpan, J.T.; Stefanopoulou, A.G.; Peng, H. Chapter three-fuel cell system model: Fuel cell stack. In *Control Fuel Cell Power System*; Advances in Industrial Control; Grimble, M.J., Johnson, M.A., Eds.; Springer: London, UK, 2004; pp. 31–56. [[CrossRef](#)]
31. Musio, F.; Tacchi, F.; Omati, L.; Stampino, P.G.; Dotelli, G.; Limonta, S.; Brivio, D.; Grassini, P. PEMFC system simulation in matlab-simulink® environment. *Int. J. Hydrogen Energy* **2011**, *36*, 8045–8052. [[CrossRef](#)]
32. Sankar, K.; Aguan, K.; Jana, A.K. A proton exchange membrane fuel cell with an airflow cooling system: Dynamics, validation and nonlinear control. *Energy Convers. Manag.* **2019**, *183*, 230–240. [[CrossRef](#)]
33. Springer, T.E.; Zawodzinski, T.A.; Gottesfeld, S. Polymer electrolyte fuel cell model. *J. Electrochem. Soc.* **1991**, *138*, 2334–2342. [[CrossRef](#)]
34. Burden, R.L.; Faires, J.D.; Burden, A.M. Chapter Five-Problemas de Valor Inicial Para Ecuaciones de Diferenciales Ordinarias. Available online: <https://latinoamerica.cengage.com/ls/analisis-numerico-2/> (accessed on 27 August 2020).
35. Shen, M.; Meuleman, W.; Scott, K. The characteristics of power generation of static state fuel cells. *J. Power Sources* **2003**, *115*, 203–209. [[CrossRef](#)]



© 2020 by the authors. Licensee MDPI, Basel, Switzerland. This article is an open access article distributed under the terms and conditions of the Creative Commons Attribution (CC BY) license (<http://creativecommons.org/licenses/by/4.0/>).